Dynamical Study of Impurity Effects on Bipolaron–Bipolaron and Bipolaron–Polaron Scattering in Conjugated Polymers

ARTICLE *in* THE JOURNAL OF PHYSICAL CHEMISTRY B · AUGUST 2013

Impact Factor: 3.3 · DOI: 10.1021/jp402963k · Source: PubMed

5 AUTHORS, INCLUDING:

Wiliam Ferreira da Cunha
University of Brasília
44 PUBLICATIONS **174** CITATIONS
SEE PROFILE

Pedro Henrique de Oliveira Neto
University of Brasília
28 PUBLICATIONS **154** CITATIONS
SEE PROFILE

Ricardo Gargano
University of Brasília
102 PUBLICATIONS **601** CITATIONS
SEE PROFILE

Geraldo Magela e Silva
University of Brasília
90 PUBLICATIONS **509** CITATIONS
SEE PROFILE

THE JOURNAL OF PHYSICAL CHEMISTRY B

Article

pubs.acs.org/JPCB

Dynamical Study of Impurity Effects on Bipolaron−Bipolaron and Bipolaron−Polaron Scattering in Conjugated Polymers

Luiz Antonio Ribeiro, Wiliam Ferreira da Cunha, Pedro Henrique de Oliveira Neto, Ricardo Gargano, and Geraldo Magela e Silva*

Institute of Physics, University of Brasilia, Brasilia, 70.919-970, Brazil

ABSTRACT: Combining the one-dimensional tight-binding Su−Schrieffer−Heeger (SSH) model and the extended Hubbard model (EHM), the scattering of two oppositely charged bipolarons and a bipolaron−polaron pair is investigated under the influence of impurity effects using a nonadiabatic evolution method. These novel results for bipolarons show that the oppositely charged quasi-particles scatter into a mixed state composed of bipolarons and excitons. The excitation yield depends sensitively on the strength of the applied electric field. In the presence of an impurity, the critical electric field regime for formation of a state composed by bipolarons and excitons is increased. Additionally, we were able to obtain critical values of electric fields that played the role of drastically modifying the system dynamics. These facts suggest that the scattering between bipolarons and a bipolaron−polaron pair in the presence of impurities is crucial for the understanding of electroluminescence in optoelectronics devices, such as polymer light emitting diodes.

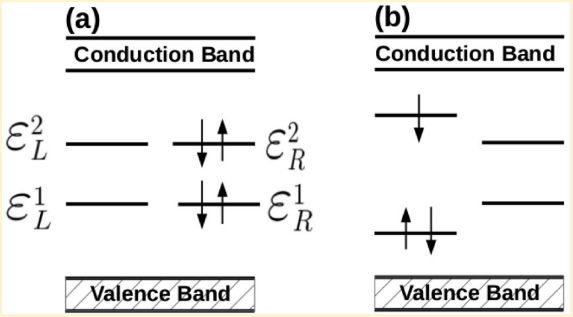

INTRODUCTION

Since the discovery of the light emitting properties on phenyl-based organic semiconductors in the 90s, a huge growth of interest in the science and technology of conjugated polymers has been observed. The electronic and optical properties of conjugate polymers, together with their mechanical properties, processing advantages, versatility of chemical synthesis, and low cost make them particularly attractive materials for the electronics industry. There are many potential applications such as organic photovoltaics devices,[1] thin-film transistors,[2] and polymer light-emitting diodes (PLEDs).[3] Especially, the characteristic to form thermally stable thin films as poly(*p*-phenylenevinylene) (PPV), which has high photoluminescence yields, makes these materials attractive for the development of PLEDs.[4,5] A PLED normally consists of a luminescent conjugate polymer layer, introduced between two metal electrodes. Electrons and holes are injected from the electrodes into the polymer layer and, as a result, this process induce self-localized electron states called polarons. A polaron has spin $\pm 1/2$ and a charge $\pm e$. It is know that the injected electrons and holes forms electron-polarons and hole-polarons due to the strong electron−lattice interactions in these materials. Bipolarons, that are spinless charge carriers and possess charge $\pm 2e$, can be created in PLEDs when the charge injection results in a large concentration of polarons. For example, two acoustic polarons with the same charge and antiparallel spins can combine with each other to for an acoustic bipolaron.[6]

When an electron-bipolaron meets a hole-bipolaron, they may collide and recombine to form a mixed state composed by bipolarons and excitons, in which the electron and the hole are bonded in a self-trapped lattice deformation known as biexciton or bipolaron−exciton, in analogy to conventional excitons in inorganic semiconductors. The photon emission results from the radiative decay of the excitations. Thus, the yield of these excitations determines the electroluminescence efficiency in conjugated polymers.[7,8] It is known that the scattering process between oppositely charged carriers and between charge carries and excitons plays an important role in the electroluminescence of PLEDs.[9−12] Also, it has been generally accepted that the electron−electron interactions and the presence of impurities in a conjugated polymer lattice critically affects the polaron and bipolaron dynamics.[13−17] Thus, the scattering process of oppositely charged bipolarons and bipolaron−polaron pair in the presence of impurities and the consequent yield of neutral excitations are believed to be of fundamental importance for PLEDs. Nevertheless, studies that take into account this physical picture remain not well described in the literature.

Another missing feature in this field of research is a complete understanding of the effects of the Hubbard type electron−electron (e−e) interactions, together with impurity effects, on the mixed state of bipolarons and excitons (biexcitons) formation. The excited polaron decay due to this kind of interaction between bipolarons and polarons is crucial for the design of more efficient devices with respect to the electroluminescence and requires a better phenomenological description.

Some relevant theoretical studies carried out by Di[18] and by Sun[19] and co-workers have shown that external electric field

Received: March 26, 2013
Revised: August 14, 2013
Published: August 16, 2013

strength has a significant influence on the results of bipolaron−bipolaron and bipolaron−polaron interactions via scattering processes in conjugated polymers. Di and collaborators used a modified version of the Su−Schrieffer−Heeger (SSH) model to include the Brazoviskii−Kirova symmetry breaking term, *e*−*e* interactions, and an external electric field to investigate the scattering and combination of oppositely charged bipolarons in a conjugated polymer monolayer and in PLED heterojunction systems. Their results show that two bipolarons can scatter into singlet biexciton state in both monolayer and/or multiple-layer electroluminescence polymeric materials. The yield of biexcitons in the collision of bipolarons can reach values as high as about 75%. The biexciton state can decay to an exciton state, which can subsequently decay to the ground state, allowing the overall electroluminescent quantum efficiency in PLEDs from all sources to reach values as high as about 75%. These results contributed to the understanding of the experimental fact that the internal quantum efficiency can reach 60%. Using a similar approach, Sun and collaborators investigated the scattering processes between a negative polaron and a positive bipolaron in a conjugated polymer chain. Their results show that, initially, the negative polaron and the positive bipolaron are accelerated by the applied external electric field. A critical electric field is found corresponding to different behavior on polaron and bipolaron collision dynamics. Below the critical electric field, the polaron and bipolaron can scatter into an excited polaron with high yield. The excited polaron can decay to the polaron state through the emission of a photon. Above the critical electric field, the polaron and bipolaron will pass through each other and continue moving as independent entities. From these works it is possible to note that the products after the bipolaron−bipolaron and bipolaron−polaron interactions show a contribution to electroluminescence in conjugated polymers. Nevertheless, a consistent study about the products of these collisional processes, particularly concerning bipolarons as quasi-particles with respect to features that might increase the critical electric field for the formation of these excitations, had not been performed, so that further investigations are needed.

In this paper, a systematic numerical investigation of impurity effects on bipolaron−bipolaron and bipolaron−polaron scattering was performed in a *cis*-polyacetylene chain in terms of a nonadiabatic evolution method. The scattering of oppositely charged bipolarons and a bipolaron−polaron pair is investigated on a conjugated polymer chain subjected to different electric field strengths, on-site, and nearest-neighbor Coulomb interactions. Ehrenfest molecular dynamics was performed by using a one-dimensional tight-binding model including lattice relaxation. Combined with the extended Hubbard model (EHM), an extended version of the SSH model was used to include external electric fields and Brazoviskii−Kirova symmetry breaking term. The aim of this work is to give a physical picture of the products and their yields due to the scattering of a bipolaron−bipolaron and a bipolaron−polaron pair in conjugated polymers, when the electron−electron interactions and impurity effects are taken into account, and contribute to the understanding of these important processes, that may provide guidance for improving the electroluminescence efficiency in PLEDs.

METHODOLOGY

A polyacetylene chain in *cis* configuration[20] was used to study collision between oppositely charged bipolarons and polaron−bipolaron pairs under the influence of impurity effects on conjugated polymers. The overall Hamiltonian is given by

$$H_{\text{total}} = H_{\text{SSH}} + H_{ee} + H_{\text{imp}} \tag{1}$$

The first term in eq 1 is the SSH-type Hamiltonian modified to include an external electric field and the Brazovskii−Kirova symmetry-breaking, which has the following form:

$$H = -\sum_{n,s} (t_{n,n+1} C^{\dagger}_{n+1,s} C_{n,s} + hc) + \sum_{n} \frac{K}{2} y_n^2 + \sum_{n} \frac{p_n^2}{2M} \tag{2}$$

were n indexes the sites of the chain. The operator $C^{\dagger}_{n,s}$ ($C_{n,s}$) creates (annihilates) a π-electron state at the nth site with spin s; K is the harmonic constant that describes a σ bond, and M is the mass of a CH group. The parameter y_n is defined as $y_n \equiv u_{n+1} - u_n$ where u_n is the lattice displacement of an atom at the nth site. p_n is the conjugated momentum to u_n, and $t_{n,n+1}$ is the hopping integral, given by

$$t_{n,n+1} = \mathrm{e}^{-i\gamma \mathbf{A}(t)}[(1 + (-1)^n \delta_0) t_0 - \alpha y_n] \tag{3}$$

where t_0 is the hopping integral of a π-electron between nearest neighbor sites in the undimerized chain, α is the electron−phonon coupling, and δ_0 is the Brazovskii−Kirova symmetry-breaking term, which is used to take the *cis* symmetry of the polymer into account. $\gamma \equiv ea/(\hbar c)$, with e being the absolute value of the electronic charge, a is the lattice constant, and c is the speed of light. The relation between the time-dependent vector potential $\mathbf{A}$ and the uniform electric field $\mathbf{E}$ is given by $\mathbf{E} = -(1/c)\dot{\mathbf{A}}$.

The second contribution in eq 1 denotes the *e*−*e* interactions and can be written as

$$H_{ee} = U \sum_{i} \left(C^{\dagger}_{i,\uparrow} C_{i,\uparrow} - \frac{1}{2} \right) \left(C^{\dagger}_{i,\downarrow} C_{i,\downarrow} - \frac{1}{2} \right) + V \sum_{i} (n_i - 1)(n_{i+1} - 1) \tag{4}$$

where U and V are the on-site and nearest-neighbor Coulomb repulsion strengths, respectively, and $n_i = C^{\dagger}_{i,\uparrow} C_{i,\uparrow} + C^{\dagger}_{i,\downarrow} C_{i,\downarrow}$.

The last contribution in eq 1 represents the one-site impurity effects and can be written in the form

$$H_{\text{imp}} = Z_j C^{\dagger}_{j,s} C_{j,s} \tag{5}$$

Z_j is the strength of an impurity, which is located at the jth site. The parameters used here are $t_0 = 2.5$ eV, $M = 1349.14$ $eV \times fs^2/Å^2$, $K = 21$ $eVÅ^{-2}$, $\delta_0 = 0.05$, $\alpha = 4.1$ $eVÅ^{-1}$, $a = 1.22$ Å, and a bare optical phonon energy $\hbar\omega_Q = \hbar(4K/M)^{1/2} = 0.16$ eV. These values have been used in previous simulations and are expected to be valid for conjugated polymers in general.[21−23]

In order to solve these equations numerically, first a stationary state that is self-consistent with all degrees of freedom of the system (the lattice plus electrons) is obtained. Then, the time evolution of the system is described by the equations of motion. The electronic wave function is the solution of the time-dependent Scrhödinger equation:

$$i\hbar\dot{\psi}_{k,s}(i,t) = -[t^{*}_{i,i+1} + V\tau_s(i,t)]\psi_{k,s}(i+1,t) - [t_{i-1}, i + V\tau^{*}_s(i-1,t)]\psi_{k,s}(i-1,t) + \left\{U\left[\rho_{-s}(i,t) - \frac{1}{2}\right] + Z_j + V\sum_{s'}[\rho_{s'}(i+1,t) + \rho_{s'}(i-1,t) - 1]\right\}\psi_{k,s}(i,t) \quad (6)$$

where k is the quantum number that specifies an electronic state,

$$\rho_s(i,t) = \sum_k{}' \psi^{*}_{k,s}(i,t)\psi_{k,s}(i,t) \quad (7)$$

and

$$\tau_s(i,t) = \sum_k{}' \psi^{*}_{k,s}(i+1,t)\psi_{k,s}(i,t) \quad (8)$$

The equation of motion that describes the site displacement and provides the temporal evolution of the lattice is obtained by a classical approach.[20] The nuclear dynamics is made with the Euler–Lagrange equations

$$\frac{\mathrm{d}}{\mathrm{d}t}\left(\frac{\partial\langle L\rangle}{\partial\dot{u}_n}\right) - \frac{\partial\langle L\rangle}{\partial u_n} = 0 \quad (9)$$

where

$$\langle L\rangle = \langle T\rangle - \langle V\rangle \quad (10)$$

Equation 9 leads to

$$M\ddot{u}_n = F_n(t) \quad (11)$$

with

$$F_n(t) = M\ddot{u}_n = -K[2u_n(t) - u_{n+1}(t) - u_{n-1}(t)] + \alpha[B_{n,n+1} - B_{n-1,n} + B_{n+1,n} - B_{n,n-1}] \quad (12)$$

where, $F_n(t)$ represents the force on the nth site. Here,

$$B_{n,n'} = \sum_{k,s}{}' \psi^{*}_{k,s}(n,t)\psi_{k,s}(n',t) \quad (13)$$

is the term that couples the electronic and lattice solutions. The primed summation represents a sum over the occupied states. By introducing instantaneous eigenstates, the solutions of the time-dependent Scrhödinger equation can be put in the form[24]

$$\psi_{k,s}(n,t_{j+1}) = \sum_l [\sum_m \phi^{*}_{l,s}(m,t_j)\psi_{k,s}(m,t_j)] \times e^{(-i\varepsilon_l\Delta t/\hbar)}\phi_{l,s}(n,t_j) \quad (14)$$

$\{\phi_l(n)\}$ and $\{\varepsilon_l\}$ are the eigenfunctions and the eigenvalues of the electronic part for the Hamiltonian at a given time t_j. Equation 12, which govern the evolution of system, may be numerically integrated using the method[24]

$$u_n(t_{j+1}) = u_n(t_j) + \dot{u}_n(t_j)\Delta t \quad (15)$$

$$\dot{u}_n(t_{j+1}) = \dot{u}_n(t_j) + \frac{F_n(t_j)}{M}\Delta t \quad (16)$$

Hence, the electronic wave functions and the lattice displacements at the $(j+1)$th time step are obtained from the jth time step. At time t_j the wave functions $\{\psi_{k,s}(i,t_j)\}$ can be expressed as a series expansion of the eigenfunctions $\{\phi_{l,s}\}$ at that moment:

$$\psi_{k,s}(i,t_j) = \sum_{l=1}^{N} C^{s}_{l,k}\phi_{l,s}(i) \quad (17)$$

where $C^{s}_{l,k}$ are the expansion coefficients. The occupation number for eigenstate $\phi_{l,s}$ is

$$\eta_{l,s}(t_j) = \sum_k{}' |C^{s}_{l,k}(t_j)|^2 \quad (18)$$

$\eta_{l,s}(t_j)$ describes the redistribution of electrons among the energy levels.

RESULTS

We carry out a systematic numerical investigation on impurities effects and e–e interactions influence over the collision dynamics of bipolaron–bipolaron and bipolaron–polaron pairs in systems composed of 200-site *cis*-polyacetylene chain. For the electric field, turned on quasi-adiabatically, the values used in the simulations varied from 0.1 to 1.0 mV/Å with a increment of 0.1 mV/Å and from 1.0 to 2.5 mV/Å with a increment of 0.5 mV/Å, whereas the on-site e–e interactions values considered are 0.1, 0.2, 0.3, 0.4, and 0.5 eV. The nearest-neighbor Coulomb repulsion strength was defined using the relation $V = U/2$. In this context, Figure 1 presents the schematic diagram of energy-levels for the configurations investigated: bipolaron–bipolaron and bipolaron–polaron pair. In Figure 1(a) we have a single polymer chain containing a hole–bipolaron, represented by the absence of electrons in the ε_L levels, which yields a $+2e$ charge, and an electron–bipolaron, represented by the full occupation of the ε_R levels thus leading to a $-2e$ charge. Figure 1(b), on the other hand, represents another kind of system in which the left partially occupied levels are characteristic of a electron–polaron, whereas the right fully occupied levels represent a hole–bipolaron energy levels configuration. One can see the characteristic larger narrowing of the bipolarons energy levels when compared to those of the polaron.

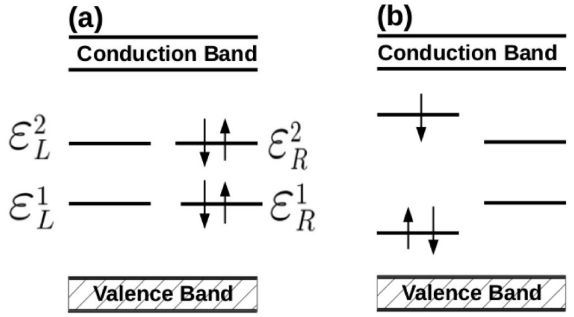

Figure 1. Energy-level schematic diagram of (a) hole–bipolaron (left) and electron–bipolaron (right) and (b) electron–polaron (left) and hole–bipolaron (right).

A number of simulations were performed in which we varied not only the kind of quasi-particle collision but also the electric field, the Hubbard interaction, and the absence or presence of the impurity. In order to better present our results, we divided this section into three subsections, each one dealing with some sort of simulation, namely the colision between bipolarons in a chain free of other defects, presented in subsection I, the influence of impurity over the bipolarons collision, in

dx.doi.org/10.1021/jp402963k | J. Phys. Chem. B 2013, 117, 11801–11811

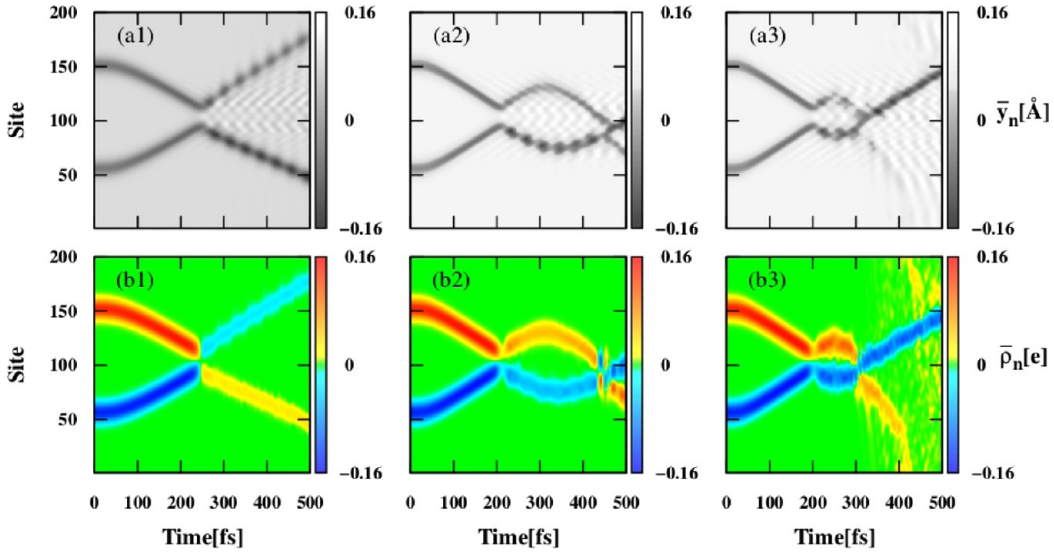

Figure 2. Bipolarons collision on a pristine chain for U = 0.1 eV. Order parameter (a) and charge density (b) time evolution. (a1−b1) 1.0 mV/Å, (a2−b2) 2.0 mV/Å, and (a3−b3) 2.5 mV/Å.

subsection II, and the polaron−bipolaron collisional process is discussed in subsection III. Also for the sake of clarity, we carry out our analysis on the quasi particles dynamics by considering the mean charge density $\bar{\rho}(t)$, derived from the charge density $\rho(t) = \sum_{k,s}{}' \psi^*_{k,s}(n,t)\psi_{k,s}(n,t)$, and the mean order parameter $\bar{y}(t)$. The expressions for these quantities are given by $\bar{\rho}(t) = 1 - [\rho_{n-1}(t) + 2\rho_n(t) + \rho_{n+1}(t)]/4$ and $\bar{y}(t) = (-1)^n[y_{n-1}(t) - 2y_n(t) + y_{n+1}(t)]/4$. The goal is to provide a better visualization of the simulations and consequently to perform a more accurate analysis of the results.

I. Bipolaron−Bipolaron Collision on Pristine Chain. We begin our discussion by considering the simulation concerning the collision between two oppositely charged bipolarons in a chain free of defect, presented in Figure 2. The upper part of Figure 2 ((a1), (a2), and (a3)) represent the order parameter time evolution. One can confirm this by noting the blurring of the figure after the collision, which is a direct manifestation of created phonons. The bottom part of the this figure, on the other hand, presents the charge density pattern ((b1), (b2), and (b3)) . As the color scale shows, we have a positive (red) structure initially in site 150 and a negative (blue) particle in the 50th site. The electric field brings the structures together and a collision takes place at varying time, depending on the applied field. This mechanism and the labeling notation is repeated throughout this work for different simulations.

In the present set of simulations we consider a Hubbard interaction of 0.1 eV and different electric fields: 1.0 mV/Å ((a1) and (b1)), 2.0 mV/Å in ((a2) and (b2)) and 2.5 mV/Å in ((a3) and (b3)). The bipolaron dynamics before the collision processes is quite similar to the polaron motion described by Stafström.[25] The first interesting feature noted by an overall view of Figure 2 is the fact that, for these regimes, the bipolarons always passes through each other after the collision. This behavior is not observed when a collisional process of a polaron-pair are taken into account, for in those systems the polaron-pair is annihilated for electric fields greater than 1.2 mV/Å.[12] We can note that the least energetic situations of Figure 2(a1) and Figure 2(b1) correspond to a scattering process. It is important to comment on, however, the difference between the emerging structures after the collision. It is noted, in Figure 2(b1), that the negatively charged excitation has a greater mobility than the positive one. This feature is to be further exploited, and can be more clearly understood in terms of a occupation number analysis, to be addressed shortly in this subsection. Another characteristic of the simulation performed in this case, that justifies this interesting and unexpected behavior, is the fact that a small value of impurity (−0.02 eV) was used in 150th site to facilitate the composition of a oppositely charged bipolaron system. The impurity causes a small difference between the charge coupled to the bipolaron lattice defects, decreasing the charge concentration in the electron−bipolaron deformation. As a result, this reduction makes the structure to be faster. It should be noted that, even thought the presence of this impurity was only meant to generate the initial negative bipolaron solution, its effect lingers throughout the whole simulation. As a consequence we obtain a positive bipolaron with a slightly lower absolute charge than the corresponding negative one. The fact that these bipolarons are not identical reflects on the difference on the dynamical behavior of the structures. Particularly after the collision, when the presence of the phonon modes helps enhancing the difference on the structure trajectories, one can see that their paths are not perfectly mirrored. Also, depending on the applied electric field, more than one collision is necessary to accomplish this dynamics (Figure 2(b2) and Figure 2(b3)). In fact, a greater level of bipolarons interaction is perceived in these cases in which the electric field and the Hubbard interaction level are sufficiently large to partially overcome the large particles inertia, creating a transition structure that is momentarily self-trapped around 100th site for about 200 fs in the case of the simulation with 2.0 mV/Å and about 100 fs for 2.5 mV/Å. Thus, we believe that after the conditions for creating this transition structure is achieved (which was not the case only for 1.0 mV/Å of Figure 2(a1) and Figure 2(b1)), the electric field tends to destabilize such structure, and to direct the system to the final state of one bipolaron passing through each other. The obtained result show that, although of similar nature, the simulation in Figure 2(a2) and Figure 2(a3) possess as products different structures: whereas in the former case, both original structures are present, in the latter, only the electron−bipolaron remains stable.

dx.doi.org/10.1021/jp402963k | J. Phys. Chem. B 2013, 117, 11801−11811

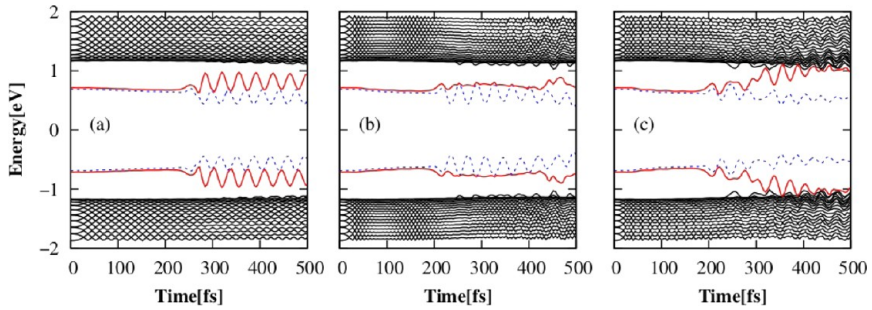

Figure 3. Energy levels time evolution for the bipolarons collision in a pristine chain for the cases showed in (a) Figure 2(a), (b) Figure 2(b), and (c) Figure 2(c).

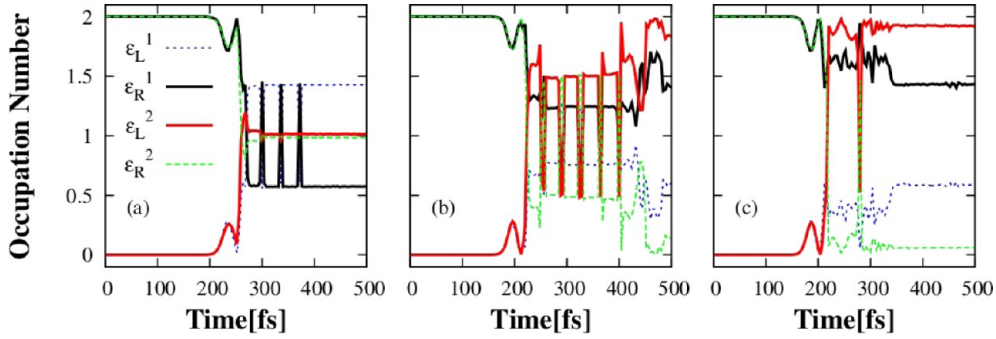

Figure 4. Occupation number time evolution for the bipolarons collision in a pristine chain for the cases showed in (a) Figure 2(a), (b) Figure 2(b), and (c) Figure 2(c).

Although we have just found a regime in which the quasi-particles destabilization is achieved, it is important to stress the great level of stability presented by the bipolaron themselves. Figure 3 presents the bipolarons energy levels time evolution for the cases presented in Figure 2. Although one can again note the oscillation pattern associated with the phonons after the collision, the presence of the states deep inside the energy gap is representative of the bipolaron integrity in Figure 2(a) and Figure 2(b). The disappearing of the structure in Figure 2(a3), corresponding to the blurring of Figure 2(b3) is an indication of the destabilization of the hole-bipolaron through the charge spread at the end of the simulation. The same feature can be exactly inferred by analyzing the red energy levels that returns to the valence and conduction band in Figure 3(c), thus conducting to the vanishing of the bipolaron. It is important to remark that previous similar theoretical work performed on polarons have not yielded equivalent results in terms of the consistency of the quasi-particle, in the sense that polarons could not survive collisions such as those implemented in Figure 2(b).[12] These considerations are consistent with the well-known fact that bipolarons are much more stable quasi-particles than polarons in conducting polymers.

Figure 4 presents the time evolution of the occupation numbers also for the cases presented in Figures 2 and 3. The fast and periodic exchange of levels between the electrons of levels ε_L^1 and ε_R^1 and between ε_L^2 and ε_R^2 is noted and might be considered to be an indication of the creation of different quasi-particles. However, these oscillations do not give rise to an amount of shift in the energy levels of sufficient magnitude to define an independent particle. The partial transference of electrons is noted by the fractional numbers achieved in the final states, which is a measure of the interference among each bipolarons electronic states. The exception stands for Figure 4(a), in which the structures pass through each other directly. The occupation numbers of Figure 4(a), suggest that both bipolarons remain stable after the collision. Even in this case, the oscillation pattern of these structures is a mere reflex of the phonons interaction that does not lead to the creation of a different particle. This conclusion is obtained through the analysis of a single electron occupying the lower levels inside the gap and some quantity near 1.5 electrons populating the levels deeper inside the gap. The difference on the kinematic behavior of the blue and red excitations in Figure 2 should be addressed for the difference in nature of these emerging quasi-particles. Concerning Figure 4(b,c), it is particularly interesting to observe the time length difference on the oscillating pattern of electrons level population, which is consistent to the lifetime of the transition structure previously mentioned. Although of similar nature, the results obtained in Figure 4(b,c) allow us to conclude that in the latter case, the creation of a neutral excitation derived from the bipolarons collision is fully accomplished.

It is important to mitigate the possible misleading feature that the scattering of bipolarons would always take place in this kind of simulation. Figure 5 presents the situation where simple scattering does not arise from bipolarons interaction. We considered an electric field and a Hubbard interaction of 0.5 mV/Å and 0.2 eV in Figure 5(a) and of 2.5 mV/Å and 0.4 eV, in Figure 5(b) respectively. The mechanics of the collision is the same as in the other simulations. In this case, however, the bipolarons are not suitably scattered. In Figure 5(a), the electric field is way too small to provide an effective collision in terms of bipolarons transference. We thus observe an approximately elastic collision between the bipolarons. In Figure 5(b), on the other hand, the collision gives rise to a neutral excitation, instead of the conventional scattering. Thus, instead of a typical collision as those proposed in Figure 2, we have the formation

dx.doi.org/10.1021/jp402963k | J. Phys. Chem. B 2013, 117, 11801−11811

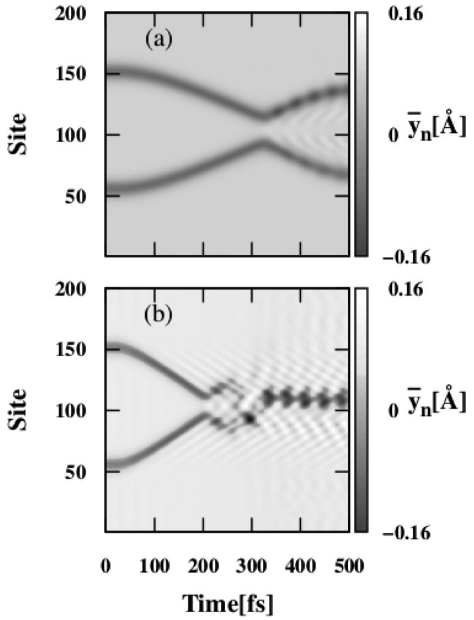

Figure 5. Order parameter time evolution in the cases: (a) Elastic collision between bipolarons for 0.5 mv/Å and U = 0.2 eV and (b) biexciton formation for 2.5 mV/Å and U = 0.4 eV.

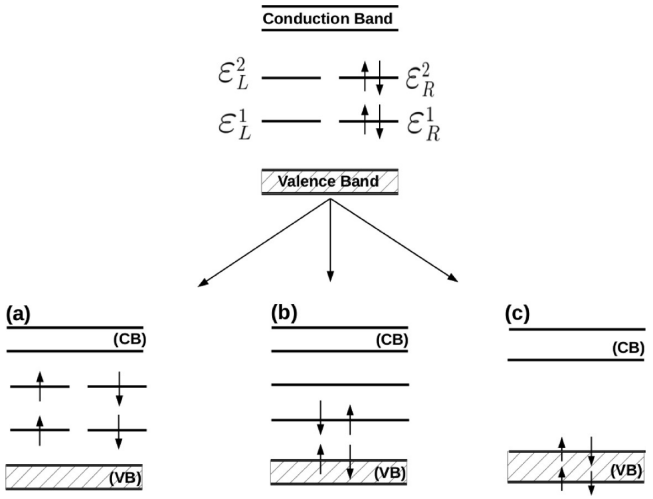

Figure 6. Possible results due to the collisional process of oppositely charged bipolarons. The conduction and valence bands are represented by (CB) and (VB) respectively.

of a different neutral structure, henceforward denominated biexciton.[18] This can be confirmed due to the fact that the resulting structure is not carried by the external electric field after the collision. We thus conclude that the Hubbard interactions and electric field regimes are of particular importance when considering each kind of particles interaction. It is important to observe that, for U > 0.4 eV, the mechanism of bipolarons recombination dominates, as described by Sun and Stafström,[26] where the mixed start of bipolarons and excitons does not occur. Thus, in order to create a given type of structure out of a collisional process, several parameters must be carefully observed.

We finish the discussion of this subsection by presenting a schematic diagram for the energy levels that represents the products of the collisional process between the bipolaron-pair. Figure 6(a) represents the product formed by the scattering of the oppositely charged bipolarons, where two bipolaron-excitons are created. Figure 6(b) shows a case where only an excited bipolaron remains in the lattice. Due to the annihilation of one bipolaron, only two energy levels are present inside the bandgap. Finally, Figure 6(c) shows the energy level configuration when both charged bipolarons are annihilated (forming a neutral biexciton), for example, for a electric field of 2.5 mV/Å and U = 0.4 eV (case showed in Figure 5(b)). This conclusions are obtained through an analysis of the occupation numbers time evolution. It is important to remark that what at first sight might appear to be the scheme of ground state systems, as might be the case of (b) and (c) systems, is, in fact, a representation of the different excited states that the system might reach after the collision. Although the electronic occupation is that of a fundamental state, we should remember that our nonlinear excitations arise from the coupling between the electronic charge and the lattice distortion, and not solely from the former. Thus, it is clear that, after the bipolarons collision, different excited states take place, as could be observed in Figure 2, for instance, that represent charge density and order parameter time evolution. As the parameters used in all simulations discussed above are noted to dramatically change the dynamical behavior of the system, it is desired to know whether other properties such as the structural characteristic of the chain also affects the obtained results. In the next subsection we specifically deal with the role played by an impurity over the collision mechanism and the resulting structures.

II. Bipolaron−Bipolaron Collision: Impurity Effects. The first set of results presented in this subsection regards the same kind of simulation as in Figure 2, but this time with an impurity of 0.2 eV placed at the 100th site. The goal is to investigate the influence this structure has over the system. In Figure 7(a1), (a2), and (a3) we considered electric field values of 1.0, 1.5, and 2.5 mV/Å, and Hubbard interactions of 0.1, 0.2, and 0.3 eV, respectively. We can see in Figure 7(a1) and (b1) that the bipolarons passes through each other when subjected to an electric field of 1 mV/Å. This results in a decrease of the critical field for transferring the bipolarons: from the 2.0 mV/Å condition on the pristine chain case to the presently discussed situation. In Figure 7(a2) and (b2), we note that, as we increase the electric field and the Hubbard interaction, the collision tends to favor the creation of a mixed state between bipolarons and excitons, through a mechanism similar to that of a transition structure discussed in the previous subsection. Nevertheless, in this case, we can already note that the emerging structure already has the exciton nature in its absence of net charge. This feature is clear in Figure 7(a2), where the order parameter path is shown to be static, in spite of the applied electric field. If we focus in Figure 7(a3) and (b3), we can note that a structure of the Figure 7(a3) with zero net charge (Figure 7(b3)) is present in the chain after the collision, but in this case, we observe the complete vanishing of the positively charged bipolaron and a much more stabilized localized bipolaron exciton state around site 65. Overall, if these results are compared to those of Figure 2, we can see that the impurity has acted in the sense of decreasing the necessary electric field to observe a proper bipolaron-exciton creation, and also led to a proper creation instead of a simple scattering of bipolarons.

Concerning the stability of the quasi-particles throughout the process, we can analyze Figure 8 in which a time evolution of

dx.doi.org/10.1021/jp402963k | J. Phys. Chem. B 2013, 117, 11801−11811

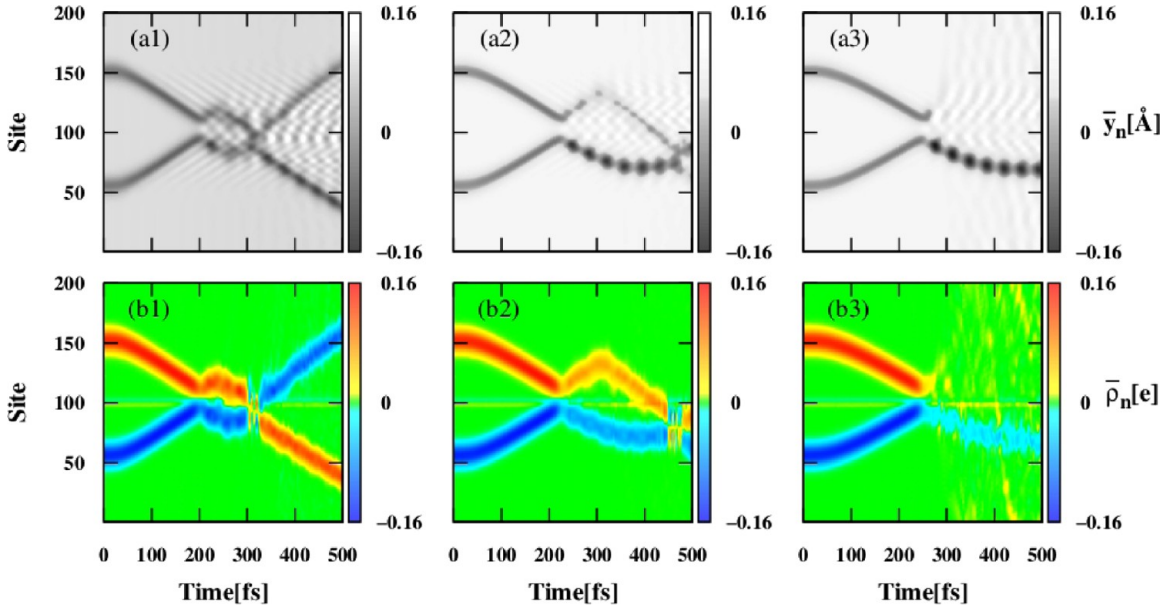

Figure 7. Bipolarons collision on an impurity (0.2 eV) doped chain. Order parameter (a) and charge density (b) time evolution. (a1−b1) 1.0 mV/Å and U = 0.1 eV; (a2−b2) 1.5 mV/Å and U = 0.2 eV; (a3−b3) 2.5 mV/Å and U = 0.3 eV.

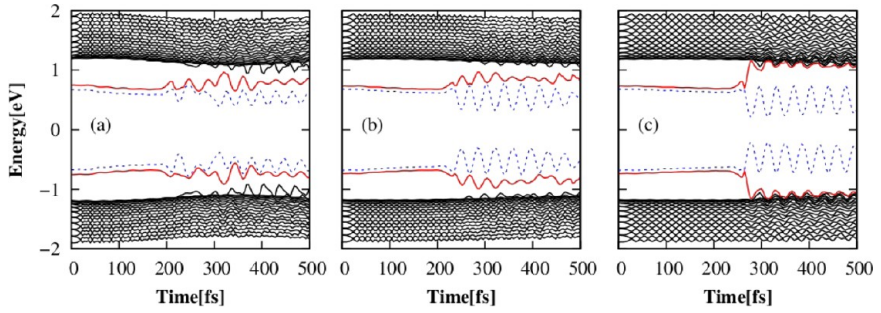

Figure 8. Energy level time evolution for the bipolarons collision in an impurity doped chain for the cases showed in (a) Figure 7(a), (b) Figure 7(b), and (c) Figure 7(c).

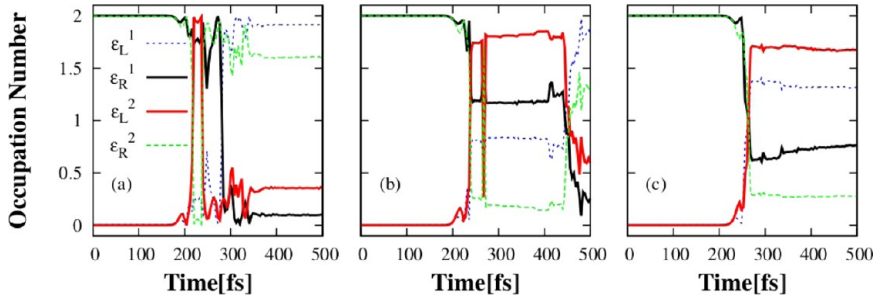

Figure 9. Occupation number time evolution for the bipolarons collision in an impurity doped chain for the cases showed in (a) Figure 7(a), (b) Figure 7(b), and (c) Figure 7(c).

the energy levels is presented. The systematic pattern of the red energy levels approaching the conduction and valence bands with the increasing of the electric field is a notorious signature of the disappearing of a bipolaron in the collisional process of excitons formation. So is the presence, albeit oscillating according to the phonon modes, of the blue levels corresponding to the other particle. Unlike Figure 8(a), Figure 8(b) and (c) shows that the mean value of the oscillating levels is importantly increased in relation to the initial value. The conclusion is that, indeed, a new particle is created out from the collision process. This conclusion is confirmed by the occupation number analysis, presented in Figure 9. The hopping between levels is diminished as the electric field is increased, due to the fact that the exciton creation is favored in these regimes. Naturally, the exchange between electrons of each bipolaron levels tends to cease when these structures are no longer available for conduction, which is definitely the case of Figure 9(c), partially for Figure 9(b) and not quite for Figure 9(a). Since the yield of exciton creation particularly depends on this oscillation frequency and of the final occupation pattern, we have found regimes in which this efficiency of creation is

dx.doi.org/10.1021/jp402963k | J. Phys. Chem. B 2013, 117, 11801−11811

higher (such as in Figure 9(c)) and others in which the efficiency is lower (such as Figure 9(a)).

At this point we should again remark that the dynamical behavior observed in Figure 2 depend intrinsically on the electric field and Hubbard parameter used in the simulations. For instance, if we use 0.5 mV/Å for the electric field and a Hubbard interaction of 0.1 eV, we reach a situation in which a bipolaron is not able to pass through each other. Figure 10 is

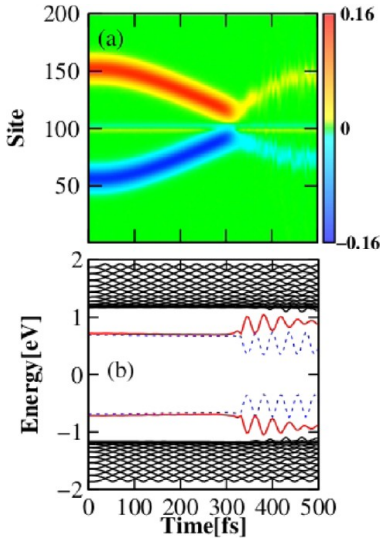

Figure 10. Bipolarons elastic collision with an impurity for 0.5 mV/Å and U = 0.1 eV: (a) charge density time evolution and (b) energy levels time evolution.

meant to discuss this possibility. In Figure 10(a) we have the charge density order parameter for the case being, whereas Figure 10(b) presents the time evolution for the energy levels. We can see what appears to be a quasi-elastic collision between the particle and the impurity. It results in the formation of a chargeless structure of the bipolaron-exciton type. The energy levels confirm this discussion through the positioning change of the particle levels inside the gap. The similarity between the results discussed for the previous case (Figure 10) to those presented in Figure 5(a) provides us with a tool to perform a fair comparison on the effects of impurity over the efficiency of the exciton creation. In order to do so, Figure 11 compares the results on occupation numbers for these situations with (Figure 11(a)) and without (Figure 11(b)) impurity on the chain. Since in both cases the bipolarons could not pass through each other, and the product is found to be of the same kind, an efficiency analysis is rather straightforward. Figure 11(a) (top) represents the occupation number analysis for the simulation in which an impurity is present in the polymer chain, whereas Figure 11(b) (bottom) is the equivalent simulation for the pristine chain. The periodic hopping of electrons between the levels is observed to be much more intense in the latter case, thus corresponding to a lower yield on the exciton efficiency. As a conclusion we have that, besides decreasing the electric field for exciton formation, another important effect impurity has over the system is to increase the efficiency of the creation these structures.

The schematic diagram for the energy levels that represents the products of the collisional process between the bipolaron-pair, in a impurity doped chain, is similar to the configurations described in Figure 6. Since the impurity endowed systems are

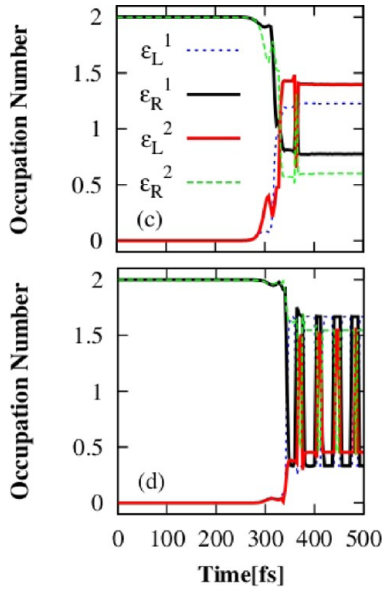

Figure 11. Bipolaron−exciton creation comparison: (a) in impurity doped chain for the case showed in Figure 10(a) (0.5 mV/Å and U = 0.1 eV) and (b) in a pristine chain for the case discussed in the previous subsection (Figure 5(a)) (0.5 mV/Å and U = 0.2 eV) .

found to be superior in every studied sense as far as the excitons study is concerned, we decided to discuss, in the last subsection, the collisional process between different types of quasi-particles, namely, polarons and bipolarons, solely considering the situation of polymer chains in the presence of impurities. The energy levels for this system configuration is represented in Figure 1(b). The products, considering the bipolaron−polaron pair collision for pristine systems, are expected to be qualitatively the same as reported in the literature,[19] when the same Hubbard and electric field parameters were applied.

III. Polaron−Bipolaron Collision. In this last subsection we discuss the results concerning the collision between a polaron and a bipolaron in an 0.2 eV impurity endowed chain. In this set of simulations we consider the collision between a electron−polaron and a hole−bipolaron. The Hubbard interaction was fixed to be 0.2 eV. Up to this point, we could observe a great deal of symmetry on the behavior of the charge carrier as a consequence of the symmetry of the used Hamiltonian. Figure 12, however, presents a very different picture. One can readily note the difference in the response between the polaron movement and that of the bipolaron. The reasoning should be obvious if we consider the difference between the masses and charges of these quasi-particles. Figure 12(a1) and Figure 12(b1) correspond to an applied field of 0.5 mV/Å. After around 450 fs, we can not observe, in Figure 12(a1), more than a single lattice distortion corresponding to a neutral complex system in Figure 12(b1). As a matter of fact, what happens is that in this regime, the structures become trapped by the impurity. Thus, in this case, instead of promoting the exciton creation, contributing to a system with better charge mobility, what happens is that the charge carriers loses their ability to follow the applied electric field, consequently yielding a system with low overall charge mobility. If we increase the electric field to the value of 1.0 mV/Å, the situation presented in Figure 12(a2) and (b2), the polaron is able to escape from the impurity potential and passes

dx.doi.org/10.1021/jp402963k | J. Phys. Chem. B 2013, 117, 11801−11811

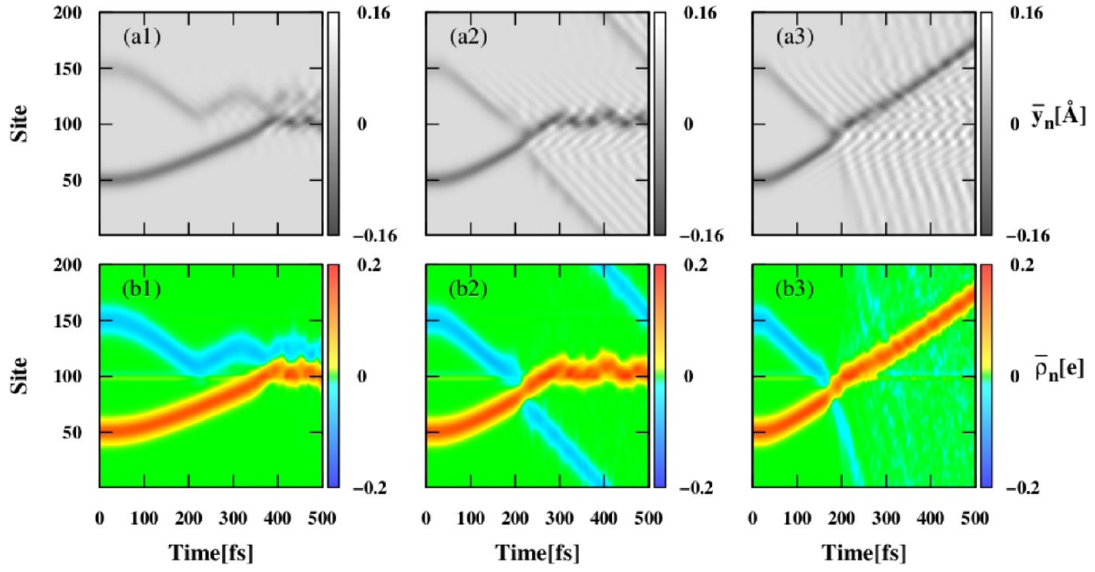

Figure 12. Polaron−bipolaron collision on an impurity doped chain for U = 0.2 eV. (a) Order parameter and (b) charge density time evolution. (a1−b1) 0.5 mV/Å, (a2−b2) 1.0 mV/Å, and (a3−b3) 2.0 mV/Å.

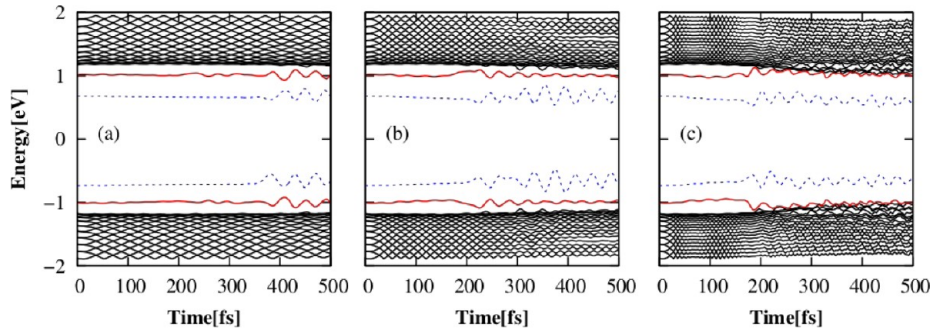

Figure 13. Energy level time evolution for the bipolaron−polaron collision in an impurity doped chain for the cases showed in (a) Figure 12(a), (b) Figure 12(b), and (c) Figure 12(c).

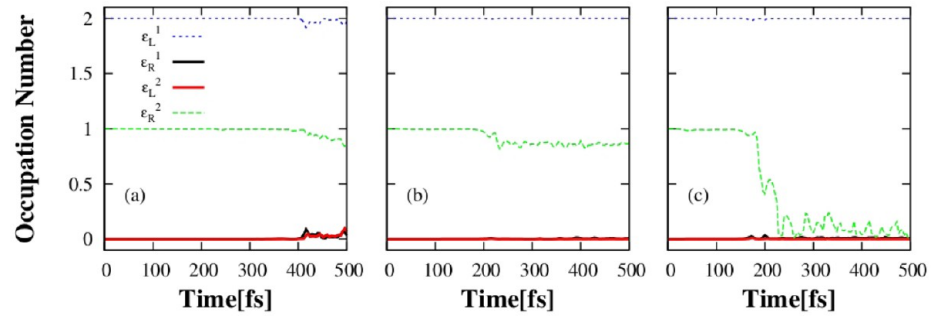

Figure 14. Occupation number time evolution for the bipolaron−polaron collision in an impurity doped chain for the cases showed in (a) Figure 12(a), (b) Figure 12(b), and (c) Figure 12(c).

through the bipolaron, which remains trapped. We can see that, even in this case, both structures remain stable both in their order parameter and in their charge density profile. A further increase on the electric field to the value of 2.0 mV/Å (Figure 12(c1) and (c2)) gives rise not only to the bipolaron release from the impurity, but also to the annihilation of the polaron, a feature that can be noted both in the order parameter and the charge density time evolution. This fact finds complete support to the already mentioned property of bipolarons being more stable structures than polarons.

Again, this analysis on the loss of stability and the kind of quasi-particle present in the system is better accomplished by studying the time evolutions of the energy levels, which is accomplished in Figure 13. The polaron levels are represented by the red lines and those of the bipolarons, by the blue lines. The aforementioned loss of stability of the polaron is observed by the reaching of the red levels in Figure 13(c) to the valence and conduction bands. This same reasoning can be obtained by studying the occupation number evolution in Figure 14. One can note in Figure 14(c) the vanishing of a polaron by the emptying of the electron in the ε_R^2 state. In this case, the

dx.doi.org/10.1021/jp402963k | J. Phys. Chem. B 2013, 117, 11801−11811

electron leaves the state inside the gap reaching the lowest unoccupied molecular orbital (LUMO), which characterizes the quasi-particle destabilization. One can observe that in Figure 13(a) and Figure 13(b), both structures are present throughout the simulation.

An interesting feature worth to discuss in the present paper is the role played by phonons in the dissociation of polarons. Figure 12 taught us that the collision carried out at such an energetic situation as a 2.0 mV/Å would lead to the polaron destruction, whereas at 1.0 mV/Å, the structure maintained its integrity. We chose to present in Figure 15 an intermediate

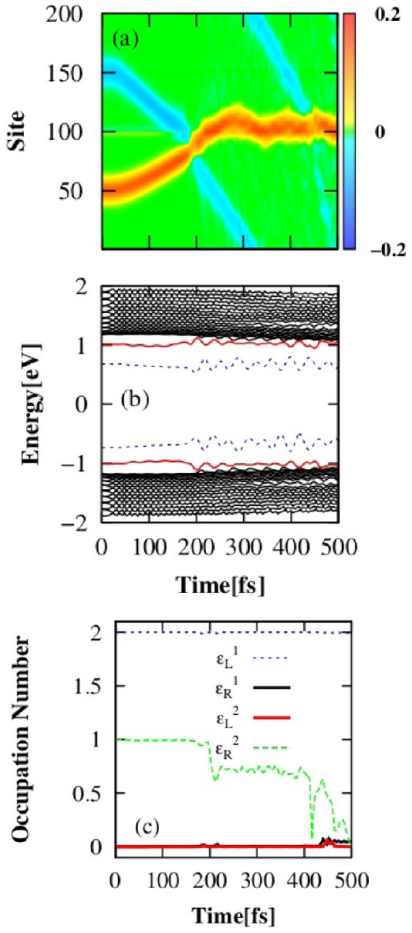

Figure 15. Multiple collisions between the bipolaron−polaron pair for 1.5 mV/Å and U = 0.2 eV. (a) charge density, (b) energy levels, and (c) occupation number time evolution.

field value of 1.5 mV/Å to investigate the effect of the collision itself on the stability of the carrier, for U = 0.2 eV. It is clear from Figure 15(a) that, in this case there are two successive collisions between the polaron and the bipolaron. It is important to note that the two collisions take place due to the periodic boundary conditions imposed to our polymer chains. By the blurring of the blue structure, one can see the relative spreading of the polaron charge after the first collision. However, the structure arises from this collision with its collective behavior unaffected. Indeed, a quick glimpse onto Figure 15(b) assures that between the two collisions, the polaron state can still be recognized. After the second collision, however, the spreading of the polaron charge is completed, as can be seen in the charge density profile of Figure 15(a) and confirmed by the returning of the polaron levels to the highest occupied molecular orbital (HOMO) and LUMO, in Figure 15(b). We conclude that the interaction with the lattice phonons created from both collisions add up to help destabilize the polaron. Another property that matches with the previous results is the integrity of the bipolaron, which remains trapped to the impurity since the first collision. All these features can be summarized by studying the occupation numbers evolution in Figure 15(c). We can recognize the disturbance of the ε_R^2 after 200 fs, when the first collision takes place, and the complete evacuation of this level after the second collision, which characterizes the polaron destruction, through the lattice vibration.

We finish our discussion by presenting a schematic diagram for the energy levels that represents the products of the collisional process between the bipolaron−polaron pair. Figure 16(a) represents the energy levels configuration of the

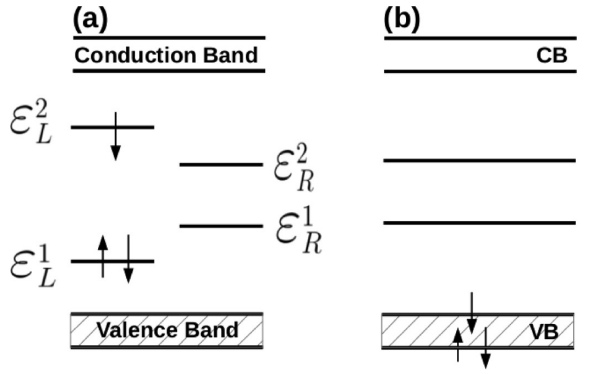

Figure 16. Possible results due to the collisional process of a bipolaron−polaron pair. The conduction and valence band are represented by (CB) and (VB) respectively.

bipolaron−polaron pair when both quasi-particles keeps the integrity. This configuration represents the cases showed in Figure 12(a) and Figure 12(b). Figure 16(b) shows a case where only a hole−bipolaron remains in the lattice. Due to the annihilation of the electron−polaron, only two energy levels (that represents a hole−bipolaron configuration) are present inside the bandgap. Such energy levels configuration represent the cases discussed in Figure 12(c) and Figure 15.

CONCLUSIONS

In summary, we developed a modified version of the SSH model to include an external electric field, the Brazovskii−Kirova symmetry breaking term, on-site and nearest-neighbor Coulomb interactions, and impurities in order to investigate the effects of these properties over the collision process of oppositely charged bipolarons and bipolaron−polaron pairs in *cis*-symmetry conducting polymers chains. Using a nonadiabatic evolution method, within a one-dimensional tight-binding model, the critical electric field regimes for formation of a mixed state compose by bipolarons and excitons was presented. The influence of electron−electron interactions on the products formed after the bipolaron−bipolaron and bipolaron−polaron collision was also discussed. Furthermore, it is found that the electron−electron interactions plays an important role on the yield of excitations after the scattering between the charge carriers in both configurations. The charge coupling to the lattice deformation after the scattering is sensitive to on-site an nearest-neighbor Coulomb interaction in the sense that, for higher values of U, less charge remains

coupled to the mixed state composed by bipolarons and excitons and the bipolaron−polaron pair. When impurity effects are taken into account, the maximum critical electric field for the formation of states composed of bipolarons and excitons increases compared to a system without impurity effects. Also, the results indicate that the presence of impurities in a conjugated polymer lattice, for all electric fields regimes, improves the excitation yield and favors the bipolaron-exciton formation. This fact may provide guidance for improving the electroluminescence yields in PLEDs.

AUTHOR INFORMATION

Corresponding Author

*E-mail: magela@fis.unb.br.

Notes

The authors declare no competing financial interest.

ACKNOWLEDGMENTS

The authors gratefully acknowledge the financial support from the Brazilian Research Councils CNPq, CAPES, and FINATEC.

REFERENCES

(1) Sun, Y.; Welch, G. C.; Leong, W. L.; Takacs, C. J.; Bazan, G. C.; Heeger, A. J. Solution-processed small-molecule solar cells with 6.7% efficiency. *Nat. Mater.* **2012**, *11*, 44−48.

(2) Braga, D.; Erickson, N. C.; Renn, M. J.; Holmes, R. J.; Frisbie, C. D. High-transconductance organic thin-film electrochemical transistors for driving low-voltage red-green-blue active matrix organic light-emitting devices. *Adv. Funct. Mater.* **2012**, *22*, 1623−1631.

(3) Lu, L. P.; Kabra, D.; Friend, R. H. Barium hydroxide as an interlayer between zinc oxide and a luminescent conjugated polymer for light-emitting diodes. *Adv. Funct. Mater.* **2012**, *22*, 4165−4171.

(4) Burroughes, J. H.; Bradley, D. D. C.; Brown, A. R.; Marks, R. N.; Mackay, K.; Friend, R. H.; Burns, P. L.; Holmes, A. B. Light-emitting diodes based on conjugated polymers. *Nature* **1990**, *347*, 539−541.

(5) Ho, P. K. H.; Kim, J. S.; Burroughes, J. H.; Becker, H.; Li, S. F. Y.; Brown, T. M.; Cacialli, F.; Friend, R. H. Molecular-scale interface engineering for polymer light-emitting diodes. *Nature* **2000**, *404*, 481−484.

(6) Di, B.; Meng, Y.; Wang, Y. D.; Liu, X. J.; An, Z. Formation and evolution dynamics of bipolarons in conjugated polymers. *J. Phys. Chem. B* **2011**, *115*, 964−971.

(7) Braun, D.; Heeger, A. J. Visible light emission from semiconducting polymer diodes. *Appl. Phys. Lett.* **1991**, *58*, 1982−1984.

(8) Köhler, A.; Wilson, J. S.; Friend, R. H. Fluorescence and phosphorescence in organic materials. *Adv. Mater.* **2002**, *14*, 701−707.

(9) Sun, Z.; Liu, D. S.; Stafström, S.; An, Z. Scattering process between polaron and exciton in conjugated polymers. *J. Chem. Phys.* **2011**, *134*, 044906−5.

(10) Sun, Z.; Li, Y.; Li, D. S.; An, Z.; Xie, S. Scattering processes between bipolaron and exciton in conjugated polymers. *Phys. Rev. B.* **2009**, *79*, 201310−4.

(11) Li, Y.; Gao, K.; Sun, Z.; Yin, S.; Liu, D. S.; Xie, S. J. Intrachain polaron motion and geminate combination in donor-acceptor copolymers: Effects of level offset and interfacial coupling. *Phys. Rev. B* **2008**, *78*, 014304−13.

(12) An, Z.; Di, B.; Wu, C Q. Inelastic scattering of oppositely charged polarons in conjugated polymers. *Eur. Phys. J. B* **2008**, *63*, 71−77.

(13) Yan, Y. H.; An, Z.; Wu, C. Q. Dynamics of polaron in a polymer chain with impurities. *Eur. Phys. J. B* **2004**, *42*, 157−163.

(14) Harigaya, K.; Terai, A. Metal-insulator transition in doped conjugated polymers: Effects of long-ranged Coulomb potentials. *Phys. Rev. B* **1991**, *44*, 7835−7843.

(15) Harigaya, K.; Wada, Y.; Fesser, K. Impurity distribution and electronic states in doped conjugated polymers in the coherent-potential approximation. *Phys. Rev. B* **1990**, *42*, 11303−11309.

(16) Di, B.; An, Z.; Li, Y. C.; Wu, C. Q. Effects of e−e interactions on the dynamics of polarons in conjugated polymers. *Eur. Phys. Lett.* **2007**, *79*, 17002−5.

(17) Zhao, H.; Chen, Y. G.; Zhang, X. M.; An, Z.; Wu, C. Q. Correlation effects on the dynamics of bipolarons in nondegenerate conjugated polymers. *J. Chem. Phys.* **2009**, *130*, 234908−4.

(18) Di, B.; Meng, Y.; Wang, Y. D.; Liu, X. J.; An, Z. Electroluminescence enhancement in polymer light-emitting diodes through inelastic scattering of oppositely charged bipolarons. *J. Phys. Chem. B* **2011**, *115*, 9339−9344.

(19) Sun, Z.; Li, Y.; Liu, D. S.; An, Z.; Xie, S. Dynamical study of polaron−bipolaron scattering in conjugated polymers. *Org. Elec.* **2010**, *11*, 279−284.

(20) Hegger, A. J. Nobel Lecture: Semiconducting and metallic polymers: Generation of polymeric materials. *Rev. Mod. Phys.* **2001**, *73*, 681−700.

(21) Ribeiro, L. A.; de Oliveira Neto, P. H.; da Cunha, W. F.; Roncaratti, L. F.; Gargano, R.; da Silva Filho, D. A.; e Silva, G. M. Exciton dissociation and charge carrier recombination processes in organic semiconductors. *J. Chem. Phys.* **2011**, *135*, 224901−5.

(22) Ribeiro, L. A.; de Oliveira Neto, P. H.; da Cunha, W. F.; Gargano, R.; e Silva, G. M. Predicting the equilibrium structure of organic semiconductors with genetic algorithms. *Chem. Phys. Lett.* **2013**, *555*, 168−172.

(23) Ribeiro, L. A.; de Oliveira Neto, P. H.; da Cunha, W. F.; e Silva, G. M. Dynamics of Photogenerated Polaron-Excitons in Organic Semiconductors. *Phys. Proc.* **2012**, *28*, 112−116.

(24) Lima, M. P.; e Silva, G. M. Dynamical evolution of polaron to bipolaron in conjugated polymers. *Phys. Rev. B.* **2006**, *74*, 224304−6.

(25) Stafström, S. Electron localization and the transition from adiabatic to nonadiabatic charge transport in organic conductors. *Chem. Soc. Rev.* **2010**, *39*, 2484−2499.

(26) Sun, Z.; Stafström, S. Bipolaron recombination in conjugated polymers. *J. Chem. Phys.* **2011**, *135*, 074902−7.